Available online at www.sciencedirect.com

SciVerse ScienceDirect

Solar Energy 86 (2012) 2802–2810

SOLAR ENERGY

www.elsevier.com/locate/solener

A full 3^4 factorial experimental design for efficiency optimization of an unglazed transpired solar collector prototype

Messaoud Badache, Stéphane Hallé *, Daniel Rousse

Technologies of Energy and Energy Efficiency Industrial Research Chair (t3e), École de Technologie Supérieure, Université du Québec, 1100 Notre-Dame St. West, Montreal, Canada H3C 1K3

Received 21 November 2011; received in revised form 21 June 2012; accepted 22 June 2012
Available online 20 July 2012

Communicated by: Associate Editor Brian Norton

Abstract

The goal of this study was to model and optimize the thermal performance of an unglazed transpired solar collector (UTC) prototype using a full factorial experiment with four factors (hole diameter, absorber coating, irradiation and mass flow rate) at three levels. A quadratic polynomial model for efficiency was shown to explain 95.47% of the variance of thermal output. Residuals analysis and analysis of variance were used to validate the best-fit model. Finally, the model was optimized using response surface representations. An optimal combination of levels of the four parameters was obtained to provide a collector efficiency of 70–80%. The chosen experimental methodology provided accurate characterization of the parameters that have the greatest impact on UTC performance.

Keywords: Unglazed transpired solar collector; Factorial experiment; Optimization

1. Introduction

1.1. Solar heat recovery

Throughout history, humans have used heat from direct sunlight to dry their crops, cook their food and keep their homes warm. Today, various kinds of solar collectors are used in almost all climates to capture solar thermal energy at low cost for many thermal applications, including institutional and residential heating, and industrial processes such as food processing and wastewater treatment. Among these solar collectors, we focus here on solar air heating systems with systems based on perforated plates called unglazed transpired collectors (UTCs).

A UTC consists of a perforated, solar-energy-absorbing plate mounted typically 10–20 cm in front of a south-facing wall. When the plate is exposed to sunlight, a significant portion of the heat absorbed is transferred to the air. The air thus preheated is drawn through the perforations into the plenum (i.e. space) between the plate and the wall by means of a fan and circulated for heating applications.

1.2. A brief review of unglazed transpired collectors

Research on UTCs began in the late 1980s. These initial studies were focused on developing a theory of heat exchange with the air passing through the perforated plates (Kutscher, 1992). Their main objective was to determine the heat transfer coefficient and heat transfer effectiveness (ε_{Hx}) of the perforated plates. Collector efficiency (η_{coll}) has been defined usually in terms of ε_{Hx} (Veronique, 2008), that is, the actual temperature rise of the air as it passes through the collector, divided by the maximum possible temperature rise (Arulanandam et al., 1999). In contrast, efficiency is more properly defined as the ratio of heat recovered to total irradiation for unit surface area.

* Corresponding author. Tel.: +1 514 396 8689; fax: +1 514 396 8530.
E-mail addresses: messaoud.badache.1@ens.etsmtl.ca (M. Badache), stephane.halle@etsmtl.ca (S. Hallé), daniel.rousse@etsmtl.ca (D. Rousse).

0038-092X/$ - see front matter © 2012 Elsevier Ltd. All rights reserved.
http://dx.doi.org/10.1016/j.solener.2012.06.020

Nomenclature

A_{coll}	collector area (m^2)
A_{cs}	pipe cross section surface area (m^2)
C_p	specific heat capacity of air (J/kg °C)
D	perforation diameter (m)
D_f	degree of freedom
G_T	incident solar radiation on the collector (W/m^2)
k	thermal conductivity of air (W/m °C)
$\dot{m}$	mass flow rate of air through the collector ($kg/m^2/s$)
P	pitch of perforations (m)
R^2	coefficient of determination
SS	sum of squares
T_{amb}	ambient air temperature (°C)
T_{out}	exit air temperature (°C)
T_{abs}	average absorber plate temperature (°C)
X	control parameters

Greek symbols

α_{co}	absorber coating
β	regression coefficients
ε_{coll}	thermal emissivity of the absorber surface
ε_{Hx}	heat exchange effectiveness
ε_b	heat exchange effectiveness at the back of the plate
ε_f	heat exchange effectiveness at the front of the plate
ε_h	heat exchange effectiveness through the holes
ρ_{air}	air density (kg/m^3)
η_{coll}	collector efficiency

However, once ε_{Hx} is known, determining collector efficiency is straightforward (Van Decker et al., 2001). Subsequent research has therefore focused on finding valid expressions for ε_{Hx}. A review of the literature on this subject uncovered information on the heat transfer coefficient and effectiveness models too numerous to mention here.

The present review includes experimental and analytical models as reported by Kutscher et al. (1993) and Van Decker et al. (2001), as well as numerical models presented by Arulanandam et al. (1999), Gunnewiek et al. (2002) and Gawlik et al. (2005), to cite just a few of the most significant works.

UTC heat-loss theory was proposed originally by Kutscher (1992), who examined the major heat loss mechanisms associated with UTCs. Kutscher concluded that heat loss due to natural convection is negligible and that loss due to wind should be small for large collectors operated at typical suction velocities.

Kutscher (1994) later investigated convection ε_{Hx} for low-speed air flow through perforated plates, with and without crosswind, using three different methods, namely transient cool-down, energy balance, and the direct ΔT method. Correlations were developed to determine ε_{Hx} as well as pressure drop. It was found that in the presence of a crosswind, the angle of the holes with respect to the normal to the surface had an observable effect. Effectiveness was greater for orientations with smaller spacing in the cross-stream direction of the hole rows.

Gunnewiek et al. (1996) modeled the flow field in the plenum using a commercial CFD code. However, modeling a full-scale UTC requires some simplifications. The approach included only the plenum region and incorporated a special set of boundary conditions to model the plate and the ambient air. Their study concluded that the velocity profile in the plenum depends on whether the flow is dominated by buoyancy forces or by the suction pressure created by the fan.

Arulanandam et al. (1999) studied the ε_{Hx} of UTCs using a commercial CFD software. Simulations were conducted over a quarter of a hole for a square pitch. Because of this limitation in the CFD study, it was necessary to place major restrictions on the problem statement, specifically the assumption of no-wind conditions and the exclusion of the heat transfer effect on the back of the plate.

Assuming an isothermal model, analytical and experimental studies done by Van Decker et al. (2001) showed that ε_{Hx} can be splited into three parts: back-of-plate (ε_b), front-of-plate (ε_f), and crossing the hole (ε_h).

Gawlik and Kutscher (2002) studied numerically and experimentally the wind heat loss from UTCs with sinusoidal corrugations. They used a numerical model to determine heat loss to the air stream over the plate as a function of wind speed, suction velocity and plate geometry. The test conditions used for experimental runs were used as inputs to the numerical model to determine whether it predicted convective heat loss accurately. Correlations for heat loss from the plate to the crosswind were determined for both the attached and separated flow cases.

Gawlik et al. (2005) compared the thermal performance of two plate geometries made with high and low conductivity material under several flow conditions. They concluded that the effect of plate conductivity on the thermal performance of a UTC is small and that low-conductivity material can be used with negligible drop in performance.

Leon and Kumar (2007) presented the details of a mathematical model using heat transfer expressions for the collector components and empirical relationships for estimating the various heat transfer coefficients. A parametric study was carried out for a wide range of designs and operating conditions. Their study concluded that solar

absorptivity, collector pitch, and air flow rate had the strongest effect on collector heat-exchange effectiveness and efficiency.

1.3. The need for an experimental design methodology

In a review of the literature published over the past 20 years, it was found (to the best of the knowledge of the authors) that the general issue of the relative influence of each parameter on UTC performance has not been discussed, despite efforts to account for most design and operationing parameters. This is most likely because evaluation and optimization of UTC thermal performance using classical experimental, analytical or numerical methods is a very complex task, given the large number of design parameters (hole diameter, pitch spacing, plate porosity, absorber coating, etc.) and operating parameters (irradiation, air suction mass flow rate, wind speed, etc.) involved. The complexity is due mainly to the multiplication of interactions between these parameters. However, these parameters and their interacting effects do not all have the same level of influence on UTC thermal performance.

A powerful and reliable decision-making method has therefore been proposed, namely the design-of-experiments method (Goupy, 2005; Montgomery, 2008; Myers et al., 2009). This method has gained a solid reputation in the field of control, modeling and optimization of complex systems. It provides the best possible information regarding parameter effects and overcomes the limitation of conventional methods by allowing evaluation of interactions between design and operationing parameters with a minimal number of measurements. The choice of this method is also motivated by the fact that its use is quite straightforward for systems that require a high number of control parameters, as is the case with UTCs. Finally, using the design-of-experiments method allows us to answer a number of questions, such as:

What is the principal parameter determining UTC thermal performance?
How might we modify this parameter to optimize performance?
How do the other parameters interact with it? Among each other?

2. The design-of-experiments method applied to a specific UTC

2.1. Objective

The design-of-experiments methodology is applied to solar collectors to determine operating conditions (of a specific UTC) that provide optimal performance and to quantify the influence of selected parameters (hole diameter, absorber coating, incident irradiation and air flow rate). More specifically, the present study presents the implementation of a three-level full factorial experimental design for the determination of a second-order polynomial model. The aim of this model being to predict collector efficiency, it should reveal the influence of the abovementioned key parameters and their interactions.

2.2. Principle of the design-of-experiments method

The principal steps that should be followed in the design-of-experiments method are shown schematically in Figs. 1 and 2 (Goupy, 2005). Fig. 1 presents the steps required to produce the planning matrix. For a successful experiment, it is crucial that potentially important parameters be identified at this stage. The next step is to specify an experimental range and a suitable level for each control parameter. This step is important because the use of an inappropriate experimental range or unsuitable parameter levels generally leads to results of poor quality and difficult to analyze (Wu and Hamada, 2009). Once all of the parameters and their experimental domains have been identified, the next step is to prepare the list of experiments to be performed. This list, also called the planing matrix, must contain all of the possible combinations of the parameters evaluated at the three levels.

Fig. 2 provides a schematic depiction of the steps required to optimize the efficiency of a UTC once the planning matrix has been obtained.

With appropriate planning, preliminary experiments can be carried out to obtain a suitable model. Once the experimental model has been determined, the optimal performance of the UTC can be predicted for the specified parameter ranges.

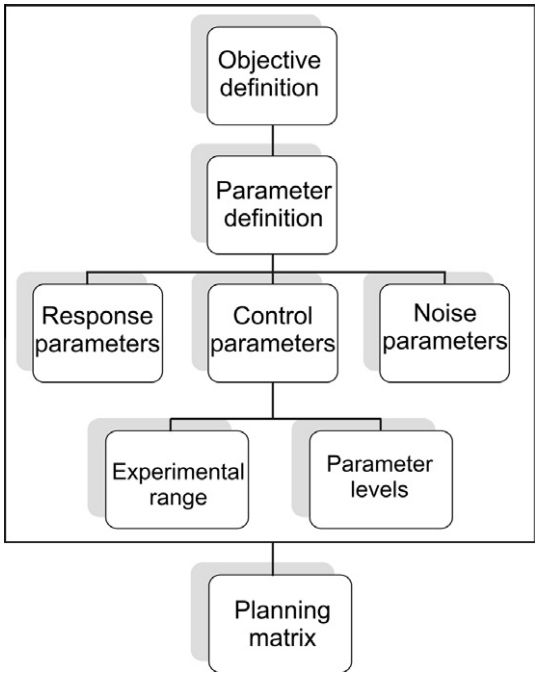

Fig. 1. Experimental design methodology applied to UTC: Schematic representation of the planning stage.

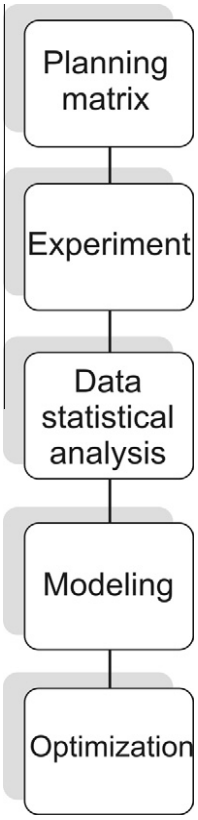

Fig. 2. Experimental design methodology applied to UTC: Schematic representation of the efficiency optimization process.

2.3. The design-of-experiments method applied to a specific UTC

Examination of the literature indicated that eleven control parameters in particular were likely to have at least some impact on the performance of a UTC. Based on preliminary tests and constraints on material and time, this number was reduced to four, namely hole diameter, (D), mass flow rate ($\dot{m}$), incident solar radiation or irradiation (G_T) and absorber coating type (α_{co}), thus simplifying the problem to be studied. Considering three levels each, we designed a complete factorial experiment with 3^4 or 81 treatments.

In the case of the proposed UTC, the first three parameters (D, $\dot{m}$ and G_T) are quantitative, while α_{co} is qualitative, since the exact value of the total hemispherical absorptivity or solar absorptivity of the collector surface was not determined at the time of the experiment. This parameter characterizes the performance of the absorber coating via the incident irradiation and emitted infrared radiation and therefore should not be confused with the total hemispherical absorptivity of the absorber.

Fig. 3 shows the various parameters identified by applying the experimental design methodology to the proposed UTC prototype described in the next section.

The response parameters that allow the prediction of UTC thermal performance are outlet air temperature (T_{out})

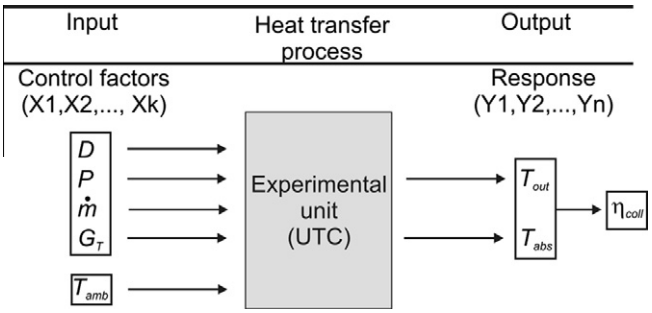

Fig. 3. Schematic representation of the experimental parameters performed on the UTC.

for efficiency and absorber temperature (T_{abs}) for effectiveness. The efficiency of a UTC is defined by the following relation (Duffie and Beckman, 2006):

$$\eta_{coll} = \frac{\dot{m}C_p(T_{out} - T_{amb})}{G_T} \quad (1)$$

The ambient temperature (T_{amb}) in the laboratory is therefore likely to have a direct influence on collector performance. In our case, this temperature was 24 ± 1 °C.

Referring to the results of Kutscher et al. (1993), the mass flow rate range was set between 0.011 kg/m^2/s and 0.040 kg/m^2/s. Several preliminary test measurements were carried out to determine the range of variation of the incident irradiation intensity (G_T), which was constrained by the intensity of the radiative heat source and the need for uniform irradiation of the absorber surface. The values considered for G_T were 348 W/m^2, 399 W/m^2 and 605 W/m^2, which corresponded to lamp-to-collector distances of 140 cm, 120 cm and 100 cm, respectively. Finally, hole diameter (D) was set between 1.5 mm (smallest) and 2.4 mm (largest), with the intermediate level set to 2 mm. Table 1 summarizes the parameters used and their levels.

The principles of experimental design require that tests be performed in random order (Wu and Hamada, 2009). However, the experiments in this study were conducted according to a preselected order due to practical constraints, in particular the difficulties associated with changing the hole diameters and the absorber coating.

3. Experimental apparatus

The experimental apparatus is composed of three main parts: the perforated collector, the air collecting and exhausting system, and the solar simulator. Fig. 4 presents a schematic representation of the experimental apparatus (Badache et al., 2010).

3.1. The perforated collector

The perforated collector was designed for vertical installation and includes the absorber plate itself, the back plate and the insulation layer. The overall size is 1.778 m × 0.60 m × 0.15 m, based on the work of Kutscher (1992).

Table 1
Parameters used and their levels.

Level	Absorber coating (α_{co})	Controls parameters		
		Diameter D (mm)	Irradiation G_T (W/m^2)	Mass flow rate $\dot{m}$ (kg/m^2/s)
Min. (−1)	Uncoated plate	1.5	348	0.011
Inter. (0)	Selective paint	2	399	0.025
Max. (1)	Black paint	2.4	605	0.039

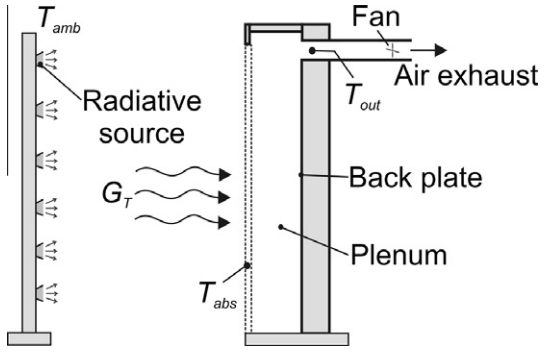

Fig. 4. Schematic representation of the experimental apparatus.

Air is drawn through a horizontal slot on the back plate into a duct in which the mass flow rate is measured. The external surface of the collector (the absorber plate) is made of galvanized steel 0.635 cm thick. The rear portion, the bottom, the top, and the sides of the apparatus are insulated with 38 mm of polystyrene foam. The overall thermal resistance is estimated at 1.2 m^2 °C/W. The whole apparatus is fastened to a wooden base designed for positioning and moving the collector while ensuring stability.

With respect to former studies (Kutscher, 1992; Van Decker et al., 2001), a triangular (staggered) pattern was chosen for the perforations, with a 24.5 mm pitch (shortest distance between two adjacent holes). Three different galvanized steel absorbers were used, the first coated with non-reflective commercially available black paint, the second with Thurmalox® 250 selective black coating (Dampney), and the third left untreated.

3.2. The ventilation system (air collection and exhaust)

The plenum thickness was 15 cm and a 75.5 L/s (160 cfm) axial inline duct ventilator (DB206) was used (Sodha and Chandra, 1994). The ventilator creates a negative pressure in the plenum, drawing heated air through the perforations at a known rate. A variable drive (3PN116B, 110/120 V, 60 Hz) ensured proper fan control. An exhaust pipe (15 cm diameter, 1.5 m length) was added to remove the heat from the unit to avoid any thermal perturbation during the experiments.

3.3. The radiative heat source (solar simulator)

Xenon long-arc lamps initially selected for their spectrum close to that of the sun would have required significant modification to laboratory security and air conditioning systems and were therefore abandoned in favor of conventional halogen lamps producing an irradiation between 300 and 700 W/m^2. The irradiation source thus consisted of a light projector fitted with 27 T3/J-TYPE/78 mm 150 W halogen bulbs collectively providing a total radiative intensity of 4.05 kW. These provided a spectrum close to that of a black body at 3500 K.

Some parameters require a high level of instrument precision, while others require certain measures concerning the installation and location of the UTC system. The European standard described by the CSTB (AFNOR, 2006) was observed to ensure proper installation of our apparatus.

3.4. Instrumentation

The instrumentation allowed us to measure the total hemispherical irradiation received by the absorber plate (G_T), the relevant temperatures (T_{amb}, T_{abs}, T_{out}), and the mass flow rate ($\dot{m}$) at the ventilation duct exit.

3.4.1. Irradiation

A Kipp&Zonen CMP11 pyranometer with a 32-junction thermopile was used to evaluate the irradiation provided by the lamps. This pyranometer, with a normal sensitivity of 9.17 μV/(W/m^2), may be used either with a multimeter or a data acquisition system. It is a class 1 instrument according to the WMO (ISO 9060). The irradiance value (G_T) can be calculated simply by dividing the output signal (U_{emf}) of the pyranometer by its sensitivity. The uncertainty of this measurement is taken as $\Delta G_T/G_T = 0.01$.

3.4.2. Mass flow rate

Hot wire anemometry (TSI, Velocicalc 8347) was used to measure air velocity. This very sensitive probe for both temperature and velocity allows measurements in the range of 0–30 m/s, with a reading uncertainty of 3% or ±0.015 m/s, whichever is greater. The typical measured velocity was about 2 m/s for the maximum pressure drop. To obtain the mass flow rate, the mean velocity $\overline{V}$ in the fully developed region of the exhaust pipe was determined from the average velocities measured at the pipe axis and several points located between the pipe axis and the solid surface. The mean velocity was then multiplied by the air density ρ_{air} at T_{out} and by the cross sectional area A_{cs}. Since the flow was fully turbulent, the velocity profile was fairly flat across the pipe section.

The uncertainty of these measurements is taken as $\Delta V/V = 0.03$. The uncertainty for ρ_{air} is assumed to be $\Delta\rho_{air}$

$\rho_{air} = 0.02$ and that of the surface area is $\Delta A_{cs}/A_{cs} = 0.01$ for a total uncertainty of the mass flow rate equal to $\Delta\dot{m}/\dot{m} = 0.04$.

3.4.3. Temperature

Three types of temperature measurement were made: ambient air temperature T_{amb}, outlet air temperature T_{out}, and absorber surface temperature T_{abs}. For each case, the temperature was measured with 29 K-type calibrated thermocouples. The uncertainty of this measurement is $\Delta T/T = 0.02$. Calibration was carried out in the 0–50 °C range. To measure T_{abs}, 24 thermocouples were bonded to the inner surface of the absorber plate at equal distances from each other (to verify the isothermal assumption). A single thermocouple in front of the unit (shielded from the lamps) was used to measure T_{amb} while another behind the unit indicated whether or not this measurement was biased by radiative flux. Two other probes measured the exhaust temperature before the fan (T_{out}) and in the fully-developed downstream exhaust zone (to estimate air density). Another probe was located in the laboratory far from the apparatus and a final probe was positioned just outside the exhaust. A complete view is given in Badache (2010).

4. Analysis of the experimental plan

Since one of the aims of this study was to establish a relationship between the four control parameters and the response of the system (η_{coll}), a second-order model that takes into account the main effects of factors and their two-factor interactions was chosen. This model can be expressed as follows:

$$Y = \beta_0 + \beta_1 X_1 + \beta_2 X_2 + \beta_3 X_3 + \beta_4 X_4 + \beta_{11} X_1^2 + \beta_{22} X_2^2 + \beta_{33} X_3^2 + \beta_{44} X_4^2 + \beta_{12} X_1 X_2 + \beta_{13} X_1 X_3 + \beta_{14} X_1 X_4 + \beta_{23} X_2 X_3 + \beta_{24} X_2 X_4 + \beta_{34} X_3 X_4 + \varepsilon_i \quad (2)$$

where ε_i is the random error component associated with the nth observation, and β_0, β_i, and β_{ij} are regression coefficients estimated by the least squares technique (Montgomery, 2008). There are fifteen coefficients, of which six refer to nonlinear interactions. Once the regression coefficients are obtained, the estimated response can be calculated easily using the model equation. In most cases, the behavior of the system is unknown, so the model must be assessed to see if it fits the experimental data. Several techniques can be used to verify model adequacy. The approach used in this study consisted of verification of model quality, adjustments to the model, and validation of the model.

4.1. Model quality

The overall predictive capability of a second-order model is commonly defined in terms of the coefficient of determination (R^2), which indicates the proportion of the total variance that is explained by the model. The coefficient of determination ranges from 0 to 1, a value approaching 1 implying that the regression model performs well. However, one must bear in mind that R^2 is not by itself a complete measurement of model accuracy (Myers et al., 2009). Checking the validity and the adequacy of the best-fit model using diagnostic tests should be done as well. The R^2 value obtained for the efficiency of the UTC was 0.9547, meaning that 95.47% of the variance is explained by the model.

4.2. Adjustments to the model

Since the model initially contains significant and non-significant terms, it can be adjusted by eliminating the non-significant terms. Draper (1998) suggested that full quadratic models should be used even if some terms are insignificant, because certain statistical properties are valid only in the full quadratic case. Myers et al. (2009) argue that reduced models containing only significant terms should be employed, especially when the goal is to find the optimal settings of major factors.

The Pareto chart in Fig. 5 shows all of the parameter effects and their interactions in decreasing order of importance. This figure uses a vertical line to determine which effects are statistically significant. The length of each bar is proportional to the value of the statistic calculated for the associated effect. Any bars beyond the vertical line are statistically significant at the selected level of significance. The (+) sign indicates a positive contribution of the effect, while the (−) sign indicates a negative contribution. In the present case, there are three main effects (A: Absorber coating, D: Flow rate, and C: Irradiation) and four significant interactions (AA, AD, AC, and DD).

The values given in Fig. 5 indicate that the effect of hole diameter (parameter B) is not significant and that all interactions involving this parameter (AB; BB; BC; BD) are negligible. The diameter effect and its interactions with other parameters may therefore be eliminated from the model. This adjustment did not affect model adequacy, since $R^2 = 0.9461$ for the reduced model remains satisfactory. The fitted model of efficiency after removing the insignificant effects is given in the following equation:

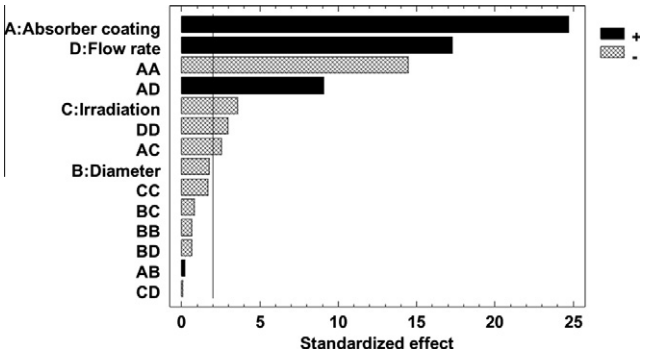

Fig. 5. Standardized Pareto chart for efficiency.

$$\eta_{coll} = 66.5 + 24.42\ \alpha_{co} - 4.29\ G_T + 18.37\ \dot{m} - 25.67\ \alpha_{co}^2 - 2.93\ \alpha_{co} \times G_T + 11.3\ \alpha_{co} \times \dot{m} - 3.92\ \dot{m}^2 \quad (3)$$

4.3. Model validation

The modeling step (next to last in Fig. 2) is concluded by validation using standard statistical tests such as residuals analysis, analysis of variance (ANOVA), Student's test or Fisher's test (Vigier, 1988). The results of the analysis of variance performed for the efficiency of the UTC (with a threshold of 95%) are presented in Table 2 for the significant parameters only. In this table, the first column is the source of the variance of the investigated or desired output η_{coll}, the second column is the treatment sum of squares of the parameter's influence (SST), the third column shows degrees of freedom (D_f), the fourth column is the mean square (column 2 divided by column 3), the fifth column shows the Fisher ratio (F-ratio) and the last column gives the P-value, here with a significance threshold of 0.05 (Vigier, 1988).

This analysis decomposes the variance of the response variable (η_{coll}) among the different factors. The values of SST and SSR (residual sum of squares) indicate whether the observed difference between treatments is real or simply experimental error. A treatment effect is significant if it exceeds the experimental error to a sufficient extent. In the present case, error (SSR = 4298.86) represents 5.7% of the total variance of efficiency ($SSTo = 74208.30$), while 94.3% of the total variance is due to treatment effects, with less than 5% probability that this distribution of variance is due to chance. This means that absorber coating, irradiation, air-flow rate plus the absorber coating × flow and absorber coating × irradiation interactions are responsible for 94.3% of the variance of the response function η_{coll} in this experiment. This confirms our initial interpretation of the effects given by the Pareto chart (Fig. 5).

Residuals are estimates of experimental errors obtained by subtracting the measured responses from the predicted responses. They can be thought of as elements of variance that are unexplained by the fitted model. In this analysis, we verify the three basic conditions (Wu and Hamada, 2009), namely independence of residuals, homogeneity of variances, and normality of residuals.

The crucial part of this step is to verify that the representation of residuals shows no particular structure for the verification of the independence of residuals and homogeneity of variances, and shows a linear pattern for the normality of residuals. After successful verification of the three basic conditions for residual analysis, it can be concluded that the model is representative and that the results obtained using it should be valid.

5. Results and discussion

The main effects plot depicted in Fig. 6 shows the estimated change in efficiency of the UTC when each of the factors is shifted from its lowest level (−1) to its highest level (+1), with all other factors held constant at 0. The plot reveals that the efficiency of the UTC decreases as irradiation increases (middle curve). This can be explained in terms of heat loss, which increases as irradiation increases. The higher the collector temperature, the higher will be the convective and radiative heat losses to the environment. This result is consistent with that reported by Leon and Kumar (2007). In addition, this graph shows that two other parameters, namely absorber coating type (left) and mass flow rate (right) have a greater effect than irradiation. The plot of each of these parameters follows a non-monotonic trend, which can be explained by the presence of terms $-25.67 \times \alpha_{co}^2$ and $-3.92 \times \dot{m}^2$ in the regression model (Eq. (3)). For irradiation and absorber coating at their mid-range levels (0), the response of efficiency to change in flow $\eta_{coll} = f(\dot{m})$ is given therefore by Eq. (4) (the curve on the right):

$$\eta_{coll} = 66.50 + 18.37\dot{m} - 3.92\ \dot{m}^2 \quad (4)$$

This plot should show a maximum located at the point where $d\eta_{coll}/d\dot{m} = 0$, which falls outside the range of variation of the mass flow rate. The mass flow rate at this point is equal to 2.34 or 0.093 kg/m^2/s. It should be noted that Eq. (4) describes the change in efficiency for air mass flow ranging between −1 and 1, that is, between 0.011 kg/m^2/s and 0.04 kg/m^2/s, and that outside this range, this expression is no longer valid because efficiency should approach a constant value as flow tends to infinity.

Table 2
Analysis of variance for the efficiency.

Source	Sum of squares (SST)	Df	Mean square	F-ratio	P-value
A: Absorber coating	31010.2	1	31010.2	526.6	0.0000
C: Irradiation intensity	1079.3	1	1079.3	18.3	0.0001
D: Air mass flow rate	18240.8	1	18240.8	309.7	0.0000
AA	11865.6	1	11865.6	201.5	0.0000
AC	337.01	1	337.0	5.7	0.0193
AD	4602.0	1	4602.0	78.1	0.0000
DD	276.6	1	276.6	4.7	0.0335
Total error	4298.8	73	58.8		
Total (corr.)	74208.3	80			

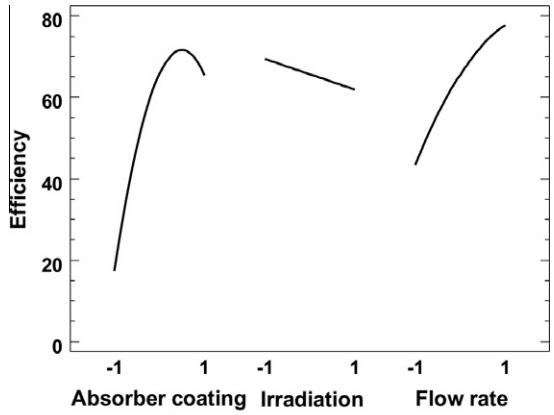

Fig. 6. Effects of the variation of the three main parameters on UTC efficiency when the other two are held constant: left – absorber coating; center – irradiation; right – mass flow rate.

The presence of a maximum in the left-side curve $\eta_{coll} = f(\alpha_{co})$ of Fig. 6 is due to the term $-25.67 \times \alpha_{co}^2$, which means that performance is strongly dependent on the type of absorber coating.

Contrary to expectation, the greatest efficiency was obtained for an optimum absorber coating level of 0.73, at which the optical properties are closer to those of a black coating than a selective coating. This may be due to the selective coating being intended for collectors exposed to solar irradiation, for which the emission spectrum is comparable to that of a blackbody at 5800 K, while halogen lamps generating an emission spectrum similar to that of a blackbody at 3500 K were used in the present study. This situation allows us to exclude the use of the selective coating and set the absorber coating level at 1 to optimize UTC performance in the presence of the irradiation source used.

Since the most influential parameters are absorber coating and mass flow rate (Fig. 5), the variation of efficiency with the type of coating was examined for the three mass flow rates.

Fig. 7 shows that changing the absorber coating from low level (−1) to medium level (0) with high-level (1) air flow increased the efficiency from 18% to 90% (top curve). However, an increase of only 27% was observed with the low (−1) air flow rate (bottom curve). The influence of mass flow rate on the efficiency of the UTC is strongly amplified when the absorber without coating (−1) is replaced by an absorber with a selective coating (0) or a black coating (1). This is consistent with experimental observations and confirms the importance of using a perforated absorber with selective or black coating (high absorptivity). In such situations, an interaction exists between these parameters, since the effect of air flow depends on the effect of the absorber coating. This interaction corresponds to the term $(11.30\,\alpha_{co} \times \dot{m})$ in the resulting model. Fig. 7 also shows that there is no significant interaction between the absorber coating and the mass flow for medium and high levels of absorber coating, since the curves are almost flat between 0 and 1 for the three cases.

6. Efficiency optimization

With the magnitude and direction of the variations of the parameters defined, the parameter settings can be optimized for collector efficiency. In the present study, response surfaces were used to obtain this information.

Fig. 8 shows the height of the response surface for efficiency over the space of the absorber coating and mass flow rate, with the other two factors (diameter and irradiation) held constant at their mid-range values.

This figure clearly indicates that the greatest efficiency was obtained at high values for absorber coating and high mass flow rates. The plot shows that several solutions are available, each with its own variability. A choice among these solutions can be made only by specifying the levels of the four model parameters. Bearing in mind that the goal of the experiment was to maximize efficiency while keeping the other factors at acceptable levels, a judicious (if not obvious) choice would be to select the black coating for the absorber, as explained above. Since hole diameter has little influence, it could be set at any value within its experimental range, based on other considerations such as manufacturing, rain or snow management. However,

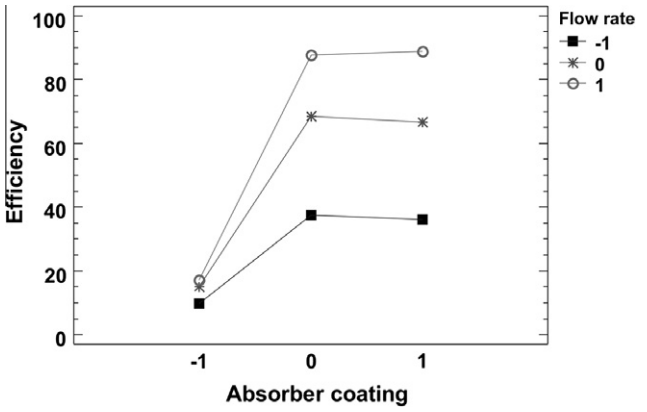

Fig. 7. Variation of the efficiency with the type of coating for the three mass flow rates.

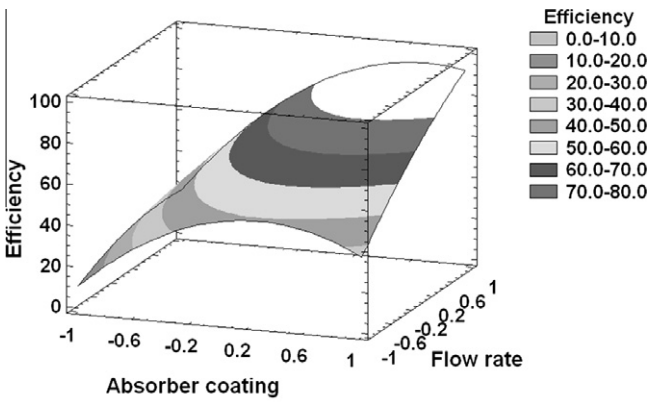

Fig. 8. Response surface for the efficiency as a function of the absorber coating and mass flow rate for fixed values of the irradiation and diameter.

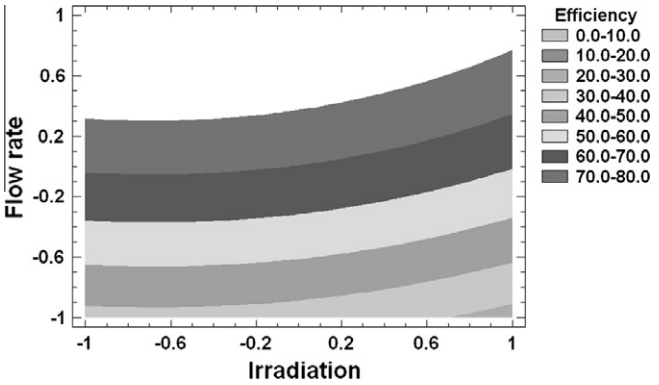

Fig. 9. Efficiency ranges as a function of the irradiation and mass flow rate for fixed values of the coating and diameter.

since hole diameter does have a slight negative impact on efficiency, the smallest diameter should be selected, which would be compatible with these other considerations. Once the absorber coating (highest) and diameter (lowest) levels are set, a contour surface plot of the efficiency of the UTC can be obtained easily.

The contour plot in Fig. 9 shows an interval for the mass flow rate between the levels "0.25" and "0.75", where the estimated efficiency is 70–80% for any irradiation G_T when D and α_{co} are set respectively at their -1 and 1 levels. This plot thus allows the detection of not only an operating point for optimal performance of the UTC, but a whole range of mass flow rates for which the estimated efficiency will range from 70% to 80%.

7. Conclusion

This paper presents the application of the design-of-experiment method for optimizing the thermal performance of unglazed transpired solar collectors (UTCs). This method has demonstrated its reliability as a tool that allows exploration of the multi-dimensional parameter spaces of complex models and helps to gain better understanding of what determines model performance. This method provided answers to several fundamental questions, such as quantifying the most sensitive parameters of the model and their interactions – a task that is difficult to perform using conventional experimental methods.

The resulting regression model has shown that the effect of hole diameter is not statistically significant (with >95% certainty), while that of irradiation is. The two main effects are contributed by the absorber coating and the mass flow rate. Finally, the response surfaces made it possible to identify the optimal set of four parameters for which the UTC efficiency ranges between 70% and 80%.

Acknowledgements

This work was supported by the t3e industrial research chair and its financial partners. The authors acknowledge their invaluable contributions. The authors are also grateful to the National Science and Engineering Research Council of Canada for a discovery Grant and two engage Grants.

References

Arulanandam, S.J. et al., 1999. A CFD heat transfer analysis of the transpired solar collector under no-wind conditions. Solar Energy 67, 93–100.

Badache, M., 2010. Modélisation et optimisation des performances thermiques d'un mur solaire a perforations (UTC). M. Ing. Ecole de Technologie Superieure (Canada), Canada.

Badache, M., Rousse, D., Halle, S., 2010. Experimental characterization of an unglazed transpired solar collector. Proc Eurosun.

Draper, NRS, H., 1998. Applied Regression Analysis (Wiley Series in Probability and Statistics).

Gawlik, K. et al., 2005. A numerical and experimental investigation of low-conductivity unglazed, transpired solar air heaters. Journal of Solar Energy Engineering 127, 153–155.

Gawlik, K.M., Kutscher, C.F., 2002. Wind heat loss from corrugated, transpired solar collectors. Journal of Solar Energy Engineering 124, 256–261.

Goupy, J., 2005. Pratiquer les Plans d'expériences, Technique et ingénierie. Série Conception. Dunod, Paris.

Gunnewiek, L.H. et al., 1996. Flow distribution in unglazed transpired plate solar air heaters of large area. Solar Energy 58, 227–237.

Gunnewiek, L.H. et al., 2002. Effect of wind on flow distribution in unglazed transpired-plate collectors. Solar Energy 72, 317–325.

Duffie, John A., Beckman, William A., 2006. Solar engineering of thermal processes. Wiley, Hoboken, N.J.

Kutscher, 1992. An investigation of heat transfer for air flow through low-porosity perforated plates. Ph.D. University of Colorado at Boulder, United States – Colorado.

Kutscher, C.F., 1994. Heat exchange effectiveness and pressure drop for air flow through perforated plates with and without crosswind. Journal of Heat Transfer (Transactions of the ASME) 116 (2), 391–399.

Kutscher, C.F. et al., 1993. Unglazed transpired solar collectors: heat loss theory. Journal of Solar Energy Engineering, Transactions of the ASME 115, 182–188.

Leon, M.A., Kumar, S., 2007. Mathematical modeling and thermal performance analysis of unglazed transpired solar collectors. Solar Energy 81, 62–75.

Montgomery, D.C., 2008. Design and analysis of experiments. John Wiley & Sons Inc.

Myers, R.H. et al., 2009. Response surface methodology: process and product optimization using designed experiments. John Wiley & Sons Inc.

Norme européenne, 2006. Installations solaires thermiques et leurs composants. NF EN 12975-2. AFNOR.

Sodha, M., Chandra, R., 1994. Solar drying systems and their testing procedures: a review. Energy Conversion and Management 35, 219–267.

Van Decker, G.W.E. et al., 2001. Heat-exchange relations for unglazed transpired solar collectors with circular holes on a square or triangular pitch. Solar Energy 71, 33–45.

Veronique, D., 2008. Analytical and Experimental Study of a PV/Thermal Transpired Collector. University of Waterloo, Waterloo.

Vigier, M., 1988. Pratique des Plans D'experiences: Methodologie Taguchi. La petite encyclopédie de la qualité. Éditions d'Organisation, Paris.

Wu, C.-F., Hamada, M., 2009. Experiments: Planning, Analysis, and Optimization, second ed. Wiley, Hoboken, N.J.